

Micrometeorological simulations to predict the impacts of heat mitigation strategies on pedestrian thermal comfort in a Los Angeles neighborhood

Mohammad Taleghani ^a, David Sailor ^b, George A. Ban-Weiss ^{a,1}

^a Department of Civil and Environmental Engineering, University of Southern California, Los Angeles, California, United States

^b Department of Mechanical and Materials Engineering, Portland State University, Portland Oregon, United States

Abstract

The urban heat island impacts the thermal comfort of pedestrians in cities. In this paper, the effects of four heat mitigation strategies on micrometeorology and the thermal comfort of pedestrians were simulated for a neighborhood in eastern Los Angeles County. The strategies investigated include solar reflective “cool” roofs, vegetative “green roofs”, solar reflective cool pavements, and increased street-level trees. A series of micrometeorological simulations for an extreme heat day were carried out assuming widespread adoption of each mitigation strategy. Comparing each simulation to the control simulation assuming current land cover for the neighborhood showed that additional street-trees and cool pavements reduced 1.5 m air temperature, while cool and green roofs provided cooling at heights above pedestrian level. However, cool pavements increased reflected sunlight from the ground to pedestrians near pavements in unshaded areas. This reflected radiation intensified the mean radiant temperature and consequently increased physiological equivalent temperature (PET) by 2.2 °C during the day, reducing the thermal comfort of pedestrians. In locations near roadways with preexisting tree cover, cool pavements caused significant reductions in surface air temperatures and small changes in mean radiant temperature during the day, leading to decreases in PET of 1.1 °C, and consequent improvements in thermal comfort. For improving thermal comfort of pedestrians during the afternoon in unshaded locations, adding street trees was found to be the most effective strategy. However, afternoon thermal comfort improvements in already shaded locations near streets were most significant for cool pavements. Green and cool roofs showed the lowest impact on the thermal comfort of pedestrians since they modify the energy balance at roof level, well above the height of pedestrians.

Key words

Heat mitigation, microclimate, outdoor thermal comfort, mean radiant temperature, cool roofs, vegetative roofs, cool pavements

¹ Corresponding author. Tel.: 213-740-9124
Email address: banweiss@usc.edu (G. Ban-Weiss)

1- Introduction

Urban areas contain about half the world's population, and 80% of the U.S. population [1]. Cities generally have higher air temperatures than their surroundings, a phenomenon known as the urban heat island effect (UHI) [2, 3]. This occurs mainly because of the replacement of natural elements such as vegetation by man-made structures and surfaces that absorb and retain sunlight. These man-made materials, such as asphalt pavements and concrete buildings, absorb and store heat from the sun due to their optical and thermal properties. They are also largely impervious to moisture and hence reduce the potential for evaporative cooling as compared to the natural surroundings. Heat also gets trapped in urban areas because of the canyon-like morphology of buildings and streets. Decreased coverage of vegetation in urban areas leads to air temperature increases from reductions in (a) "evaporative cooling" via evapotranspiration, and (b) shading of surfaces [4-6]. The heat island effect is further amplified by the emission of waste heat from energy consuming activities in cities [7-9]. UHIs can increase building energy use [10], and also affect human health and thermal comfort in urban spaces where pedestrians have no access to air conditioning systems, and consequently are prone to heat related illnesses. These illnesses range from heat edema and heat rash to heat stroke associated with neurologic dysfunction when body temperature is greater than 40.6 °C [11].

Several past studies have investigated the impacts of heat mitigation strategies on the UHI in different climates. The most common strategies are solar reflective "cool" roofs, vegetative "green roofs", solar reflective cool pavements, and increased street-level urban vegetation [12, 13]. Cool roofs and pavements reduce urban temperatures by decreasing the fraction of incoming sunlight that is absorbed and consequently transferred to the atmosphere. Green roofs and urban vegetation reduce urban temperatures by increasing evaporative heat fluxes while decreasing sensible heating. Urban vegetation can also provide shading to urban surfaces, buildings, and pedestrians. Most past studies on the impacts of heat mitigation strategies have generally investigated the mesoscale meteorological consequences of hypothetical city-wide deployments of these strategies using numerical weather prediction models [14-28]. Few studies have investigated heat mitigation strategies at the microclimate (neighborhood) scale using numerical simulations [29-34].

In a comprehensive review study, Santamouris [35] showed that city-wide urban albedo increases are associated with mean reductions in ambient air temperature of about 0.3 K per 0.1 increase in the urban albedo. Corresponding decreases in daily peak ambient temperatures

are about 0.9 K per 0.1 urban albedo increase. Cool roofs in particular were reported to decrease ambient temperatures between 0.1 and 0.33 K per 0.1 increase in roof albedo. City-wide deployment of green roofs, on the other hand, was estimated to decrease ambient temperatures by 0.3 to 3 K. In another study, Millstein and Menon [36] performed simulations to predict the climate impacts of modifying urban surface albedo in cities around the United States. They found that air temperatures in urban locations around the U.S. were reduced by 0.11-0.53 °C and 0.05-0.41 °C during summer and winter, respectively. In another study focusing on central and southern California, Taha [37] simulated 1-2 °C reductions in peak urban air temperatures after increasing surface albedo and implementing urban reforestation across the city.

Heat mitigation studies generally focus on changes to urban air temperature. However, air temperature is only one of the factors that influences human thermal comfort. Several studies have shown that outdoor thermal comfort is better associated with mean radiant temperature than air temperature [38-40]. Mean radiant temperature sums the shortwave and longwave radiation fluxes to which a body is exposed, and therefore is an important metric related to the energy balance of the human body and human thermal comfort [41, 42]. It is defined as the *'uniform temperature of an imaginary enclosure in which the radiant heat transfer from the human body is equal to the radiant heat transfer in the actual non-uniform enclosure'* [43]. Heat mitigation strategies can alter both radiative fluxes (that can be absorbed by pedestrians) and air temperature. As an example, trees in urban spaces block the sun and thus reduce mean radiant temperature in street canyons while also reducing air temperature by increasing evapotranspiration. The influence of vegetation on thermal comfort has been studied on different scales ranging from single trees to urban parks [32, 44-47]. At the scale of single trees, Lin and Lin [47] measured air and surface temperature under ten different tree types in Taipei City. They showed that air temperatures under the tree canopies were 0.6 to 2.5 °C cooler than a nearby unshaded open space, while surface-soil temperatures were 3.3 to 8.1 °C lower. At the park scale, Spronken-Smith and Oke [44] found that the cooling influence of parks in a hot climate (Sacramento, California) was 2 °C larger than in a cold climate (Vancouver, Canada). Another class of heat mitigation strategies that influence both radiative fluxes and air temperature is solar reflective materials such as cool roofs and pavements. These cool materials have lower surface temperatures and thus transfer less heat to the air, but also increase reflected sunlight. The influence of reflective materials on air temperature has been investigated in past work [19, 23-28, 35, 48-51], but to our knowledge only one study has investigated the impacts of cool surfaces on pedestrian thermal comfort [23]; they investigate

heat mitigation at the mesoscale, and so may leave out important complexities that occur at the microscale that influence thermal comfort.

In this study, we investigate the influence of different heat mitigation strategies on the microclimate of El Monte, California, located in eastern Los Angeles County (34.073 °N, 118.028 °W). The heat mitigation strategies of focus are cool roofs, cool pavements, street-level trees, and vegetative roofs. The impacts of these heat mitigation strategies on the thermal comfort of pedestrians is quantified. We implement a high resolution micrometeorological model that is capable of resolving individual buildings and the complex mixing phenomena that occurs as a result of buoyancy effects resulting from differential solar heating of roofs, exterior walls, and ground-level surfaces. Simulating the impacts of heat mitigation strategies at this scale allows for better characterizing their impact on the thermal comfort of pedestrians in urban spaces and streets. This study builds on previous work that has investigated the influence of heat mitigation strategies using mesoscale climate models. These models do not resolve some important complexities of urban environments due to their relatively low spatial resolution (typically ~1x1 km or coarser).

2- Methods

2.1 Microclimatological model

This research employs a computational fluid dynamics (CFD) model known as ENVI-met, which was initially developed in the late 1990s at the Institute for Geography in Ruhr-University, Germany [52] and is still undergoing refinements and extensions to its capabilities. ENVI-met has been validated in numerous studies for its ability to replicate thermal environmental conditions at the neighborhood scale (see the Supplementary Materials for a summary of such studies).

ENVI-met requires two types of inputs that describe (a) land cover geometries and physical properties for buildings, pavements, and vegetation (further explained in subsequent sections), and (b) meteorological boundary conditions at the edges of the domain. Simulations were performed for a hot summer day during a heat wave, July 30th, 2014.

The main atmospheric prognostic variables in ENVI-met are turbulence, wind flow, temperature, and humidity. Turbulent air flow is modeled in three dimensions using the non-hydrostatic incompressible Navier-Stokes equations with density removed using the Boussinesq

Approximation. The inflow wind profile at the boundary is prescribed (see Table 1). The lateral and outflow boundary conditions for wind use a zero-gradient Neumann condition. The boundary of all solid surfaces uses the no-slip condition.

Turbulence is simulated using a 1.5 order turbulence closure model. This model is based on Mellor and Yamada [53], but adds local turbulence and its dissipation rate as two additional prognostic variables [54],[55].

Ground surface temperatures are computed using the energy balance equation as

$$0 = R_{sw,net} + R_{lw,net} - c_p \rho J_h - \rho L \cdot J_v - G \quad (1)$$

where $R_{sw,net}$ and $R_{lw,net}$ are the net radiative fluxes of shortwave and longwave energy, J_h and J_v are the turbulent fluxes of heat and vapor, c_p and ρ are the specific heat and density of air, L is the latent heat of vaporization, and G is the soil heat flux. For building surface temperatures, G is replaced by the heat transmission through the wall and roof. Radiative fluxes are altered by buildings and plants using flux reduction coefficients [56] that resolve both direct and diffuse radiation, and parameterizes the influence of local obstructions using sky view factors derived from the ray-tracing module in the model. In equation 1, $R_{sw,net}$ is calculated as

$$R_{sw,net} = (R_{sw,dir}(z=0) \cos \beta + R_{sw,diff}(z=0)) (1 - a_s) \quad (2)$$

in which β is the angle of incidence of the incoming shortwave radiation relative to the surface exposition, a_s is the surface albedo, $R_{sw,dir}$ and $R_{sw,diff}$ are the direct and diffuse components of shortwave radiation, and $z=0$ represents the surface.

The longwave budget ($R_{lw,net}$) is split into a fraction that is unshielded by buildings ($R_{lw,net}^{us}$) and a fraction obstructed by buildings ($R_{lw,net}^s$):

$$R_{lw,net}(T_0) = \sigma_{svf} R_{lw,net}^{us}(T_0) + (1 - \sigma_{svf}) R_{lw,net}^s \quad (3)$$

where σ_{svf} is the sky view factor used to weight the energy budget for the shielded and unshielded fraction, and T_0 is the ground surface temperature. The exchange of radiation between the ground and vegetation, and ground and buildings is further described in [[57]].

The soil heat flux is calculated from equation 4 based on the surface temperature and the temperature of the first level of the soil model below the surface:

$$G = \lambda_s (k = -1) \frac{T_0 - T(k=-1)}{0.5 \Delta z (k=-1)} \quad (4)$$

where λ_s is the heat conductivity of the first soil layer (representing by $k = -1$). For buildings, G is replaced by Q_w and calculated by:

$$Q_w = k(T_w - T_{a,i}) \quad (5)$$

where k is the heat transmission coefficient of the wall model and $T_{a,i}$ is the indoor air temperature of the building.

The treatment of vegetation in ENVI-met is extensively explained in Section 4 of [52] through turbulent fluxes of heat and vapor, stomatal resistance, energy balance of the leaf, and water balance of the plant/soil system.

Boundary conditions for the control simulation are shown in Table 1. A telescoping grid for vertical layers is used where layer thickness increases with height. This somewhat limits vertical resolution at rooftop level, which may adversely impact the ability of the model to resolve rooftop mitigation strategies.

2.2 Study domain

This study focuses on a neighborhood in El Monte, California, located in Los Angeles County on the west coast of the United States. El Monte has a Mediterranean climate based on the Köppen-Geiger climate classification [58], and is influenced by the Pacific Ocean, which is 53 km to the west (Figure 1). The average daily maximum air temperature in August is 31 °C (88 °F), and average daily minimum air temperature in January is 7 °C (45 °F) [59]. As of the 2010 Census, El Monte had an average income of \$39,535. This is in contrast to a national average of \$50,502 [60]. Hence, El Monte represents a neighborhood with a particularly vulnerable population. The neighborhood of focus, which covers 450 x 650 m, was chosen as generally representative of a residential area in El Monte.

2.3 Scenarios

A total of five scenarios were simulated, each assuming different land cover in the neighborhood. The control (CO) scenario was simulated assuming current land cover, determined using Google Earth imagery (Figure 1). Most buildings in this neighborhood were observed to be detached residential homes with two stories, and back yard and front yard gardens largely covered with grass and some trees. The roads are made of asphalt concrete

and the sidewalks of cement concrete. Other surface physical characteristics and soil data are presented in Table 1s and 2s in supplementary material. The control simulation was evaluated by comparing simulated results to the nearest weather station, located at the El Monte airport [59]. Measured versus simulated surface air temperatures show a coefficient of determination of 0.91 (see the supplementary material for more detail). A series of perturbation scenarios were simulated to investigate the impacts of heat mitigation strategies on micrometeorology and thermal comfort (Table 2). In the green roof (GR) scenario, each roof was assumed to be covered with grass. We note here that not all residential roofs have the structural integrity to house a green roof. Nevertheless, our aim is to predict the maximum possible impact of these heat mitigation strategies and thus we assume hypothetically that all roofs could house green roofs. In the cool roof (CR) scenario, the albedo of all roofs is increased from 0.1 to 0.4. Cool roofing products (e.g. shingles or tiles) for residential homes with pitched roofs are currently available in the marketplace with “aged” [61] albedos of 0.4 [62]. These materials are designed to maximize reflectivity in the near-infrared part of the solar spectrum, allowing for high albedo roofs that appear relatively dark in color. In the third perturbation scenario (TA), trees were added to open grassy spaces in front yards adjacent to sidewalks (in addition to current vegetation and trees). For the cool pavement scenario (CP), the albedo of all asphalt pavement in the domain was increased by 0.3. This represents an upper bound value for what is currently technologically achievable. Wall albedo in all simulations is assumed to be 0.2.

The impacts of the four heat mitigation strategies on meteorology and thermal comfort were investigated by comparing GR, CR, TA, and CP to the control simulation (CO). We focus on micrometeorological predictions of surface air temperature, mean radiant temperature, relative humidity, and wind speed. More details on the calculation of thermal comfort are presented in the next section.

2.4 Calculation of thermal comfort

Thermal comfort is defined as “*that condition of mind which expresses satisfaction with the thermal environment*” [63]. There exist models to assess thermal perception of humans. These models use basic thermoregulatory processes (such as dilation of peripheral blood vessels and the physiological sweat rate) of the human body [39, 64]. We assess thermal comfort based on physiological equivalent temperature (PET), which is one of the most commonly used indices for outdoor thermal comfort. PET uses the Munich energy balance model for individuals (MEMI)

[64] which is a thermo-physiological heat balance model. MEMI is based on the energy balance equation for the human body:

$$M + W + R + C + E_D + E_{Re} + E_{Sw} + S = 0 \quad (6)$$

where M is the metabolic rate (internal body energy production), W is the physical work output, R is the net radiation of the human body, C is the convective heat flow, E_D is the latent heat flow to evaporate water diffusing through the body skin (imperceptible perspiration), E_{Re} is the sum of heat flows for heating and humidifying the inspired air, E_{Sw} is the heat flow due to evaporation of sweat, and S is the storage heat flow for heating or cooling the body mass.

This index considers four meteorological and two thermo-physiological parameters [65]: air temperature ($^{\circ}\text{C}$), air relative humidity (%), wind velocity (m/s), mean radiant temperature ($^{\circ}\text{C}$), thermal resistance of clothing (Clo), and level of activity of humans (W).

PET uses Predicted Mean Vote (PMV) scales (9 grades) to create a comfort index. The PMV model, developed in the 1970s for the American Society of Heating, Refrigerating and Air-Conditioning Engineers (ASHRAE), is among the most recognized thermal comfort models. PET simplifies the complexities of outdoor climate into an index with units of $^{\circ}\text{C}$. It provides the equivalent temperature of an isothermal reference environment with a 12 hPa water vapor pressure (relative humidity = 50% at 20 $^{\circ}\text{C}$) and air velocity of 0.1 m/s, at which the heat balance of a lay person is maintained with core and skin temperature equal to those under the conditions in question [65, 66]. Table 3 shows the ranges of the physiological equivalent temperature (PET) for different grades of thermal perception by human beings and physiological stress on human beings.

To calculate PET we use the RayMan model [67]. This model calculates PET based on the aforementioned six parameters given for a specific time and location. Thus, pedestrian thermal comfort was computed for each scenario at a variety of receptor locations (see red circles in Figure 1) in the neighborhood. Meteorological parameters are from the ENVI-met simulations. Assumed thermo-physiological parameters for a “normal” pedestrian are shown in Table 4. We note that computed PET is sensitive to assumed thermo-physiological parameters. Activity (a.k.a. metabolic rate) can range from 40 W/m^2 (sleeping) to 410-505 W/m^2 (wrestling) [68]. Metabolism also depends on personal attributes such as height, weight, age and gender. Clothing insulation, which affects heat exchange between the human body and surroundings ranges from 0 for a naked person to 1.5 for a person in heavy winter clothes. Note that 1 Clo =

$0.155 \text{ K m}^2 \text{ W}^{-1} = \text{R-value of } 0.88$ (United States customary units). The assumed values listed in Table 4 represent a normal person walking with summer clothes in the simulated neighborhood.

3- Results and Discussion

3.1 Impacts of heat mitigation strategies on air and mean radiant temperature

Air temperature (T_a) and mean radiant temperature (T_{mrt}) for the control simulation is presented in Figure 2. Values are for a height of 1.5 m above the ground, close to the height of the human body core. Surface air temperatures above asphalt pavements are higher than other parts of the domain. This is expected given the low albedo and lack of shading of pavements by trees in this domain. The lowest surface air temperatures correspond to locations underneath trees, a direct consequence of shading the surface. Similarly, T_{mrt} is higher in paved areas relative to shaded areas. The maximum difference in T_{mrt} for unshaded asphalt concrete roads versus shaded vegetative areas is nearly 30 °C.

Figure 3 presents differences in surface air temperature (a-d) and mean radiant temperature (e-h) for the four heat mitigation simulations versus the control simulation. Values are for afternoon at 14:00h, when surface air temperature reaches a maximum in the control simulation. Cool pavements cause significant decreases in surface air temperature, with regions above asphalt pavements cooling up to 2 °C relative to the control simulation. Adding street level trees and cool roofs also reduces surface air temperature, but to a lesser extent than cool pavements. Green roofs are simulated to have the least impact on surface air temperature. Thus, these simulations suggest that roof level heat mitigation strategies are less effective at reducing surface air temperature than street-level strategies for the neighborhood and conditions under investigation (Figure 3a-d). This is consistent with another recently published study that found little street-level effects for rooftop mitigation on buildings higher than two stories [69]. Assessing changes in mean radiant temperature at 1.5 m (Figure 3e-h) suggests that street level strategies (cool pavements and additional trees) again have more impact than roof-level strategies (cool and green roofs). Additional street trees reduces mean radiant temperature at the locations of new trees by up to 20 °C. This is due to the decrease in downwelling solar radiation that reaches the surface from tree shading. The mean radiant temperature above pavement in this scenario is nearly unchanged. In contrast, cool pavements cause an increase in mean radiant temperature above paved surfaces of up to about 7.8 °C. The increase in mean radiant temperature is driven by the increase in reflected shortwave radiation from the surface.

3.2 Impacts of heat mitigation strategies on thermal comfort of pedestrians

To assess the impacts of heat mitigation strategies on the thermal comfort of pedestrians, we begin by focusing on five unshaded receptor locations within the domain, shown in Figure 1. The receptors are located above asphalt pavements in the center and outside streets of the central block.

Figure 4 shows vertical profiles of air temperature and mean radiant temperature at 14:00 for the receptor at the center of the model domain. Vertical profiles are plotted from the surface to a height of 2.5 m, slightly above the simulated pedestrian height of 1.75 m. The addition of cool pavements reduces the air temperature of the atmospheric surface layer by about 0.8 °C relative to the control; the temperature difference decreases as height increases (Figure 4a). Street level vegetation reduces air temperature in the surface layer at this receptor by about 0.15 °C. The impact of street-level trees at this unshaded receptor is lower than it would be for a receptor underneath a newly added tree. Green and cool roofs reduce air temperature in the surface layer by about 0.2 °C. This temperature difference is similar in magnitude as height increases to 2.5 m. The impacts of heat mitigation strategies on vertical profiles of mean radiant temperature are markedly different than for surface air temperatures (Figure 4b). Cool pavements markedly increase mean radiant temperature at this receptor by around 8.9 °C at all heights considered. The other heat mitigation strategies reduce mean radiant temperature by less than 0.15 °C at this receptor location.

Thermal comfort is computed for the receptor locations shown in Figure 1b at the height of 1.5m. The diurnal variation in mean physiological equivalent temperatures for all receptors is shown in Figure 5 (separately for shaded and unshaded receptors). These calculations are performed for a walking person (80 W) wearing summertime clothing (0.5 Clo) as described in Section 2.4.

In unshaded locations (Figure 5a), PET shows a strong diurnal cycle with maximum values at 15:00. The differences in PET among the simulations are generally largest during the sunlit hours of the day, as expected. The mean PET between 05:00 and 17:00 in unshaded locations was 35.5 °C, 34.9 °C, 36.3 °C, 34.7 °C, and 37.7 °C for the control, green roof, cool roof, street trees, and cool pavement scenarios, respectively. Thus, the implementation of cool pavements result in the highest values of PET and street trees result in the lowest values in these unshaded receptor locations. On the other hand, after 17:00, the cool pavement simulations

result in the lowest values for PET. This can be explained by the fact that (a) solar radiation and therefore reflected solar radiation is small after 17:00 and zero after sundown, and (b) surface air temperatures are reduced compared to the control given the lower absorbed solar radiation throughout the day. (For reference, the sunset on July 30th is at 19:56.) In summary, street trees and green roofs were the most effective strategies for reducing PET in unshaded locations in the domain during sunlit hours, while cool pavements were the most effective after sundown (mainly because cool pavements with high albedo store less heat during the day and consequently release less at night).

To explore how shading impacts the effect of heat mitigation strategies on pedestrian thermal comfort, PET was also calculated underneath street trees in each scenario (Figure 5b). Note that the receptors were located underneath preexisting trees, not new trees added in the 'TA' scenario (see Figure 1), and above grass near roads, but not on roads. As with the unshaded receptors, the maximum PET for the shaded locations occurred at 15:00. The maximum PET among the scenarios occurred for the control and cool roof scenarios (39.6 °C at 15:00), while the minimum PET was simulated in the cool pavement scenario (11.3 °C at 4:00). In general, the mean PET between 05:00 and 17:00 in shaded locations was 21.9 °C, 21.8 °C, 21.9 °C, 20.9 °C, and 20.8 °C for the control, green roof, cool roof, street trees, and cool pavement scenarios, respectively. Thus, adding street trees and cool pavements were the most effective heat mitigation scenarios for reducing PET in shaded receptor locations (under trees that existed in all scenarios including the control). Also, note that adding cool pavements increased PET by 2.2 °C in unshaded regions (as explained in the previous paragraph), but decreased PET by 1.1 °C in shaded areas. These decreases in PET in shaded areas, which are near (but not above) pavements, stem from (a) reductions in surface air temperatures from air that has been advected from above pavements to the shaded receptors, in conjunction with (b) small changes in mean radiant temperature at the shaded receptors during the day. In other words, the air temperature effect overwhelms the radiative effect.

To further investigate the effect of shading on thermal comfort, PET was compared near the center of the domain in the control scenario in a shaded (with tree) and unshaded location (Figure 6). After sunrise at 06:00, PET in the unshaded location increases markedly. The maximum PET at this location reaches 48.3 °C at 15:00. PET in the shaded location at this time of day is 41.0 °C, illustrating the importance of increasing shade for improving PET. PET in the two locations nearly converge after 17:00.

PET for unshaded and shaded receptor locations at the center of the domain is shown in Figure 7 for each simulation. Values are for 15:00, the time at which maximum PET occurs (Figure 6). The difference in shaded and unshaded PET is about 7 °C for all simulations other than ‘CP’, which has a corresponding difference of 12.7 °C. The shaded location in the cool pavement scenario has a lower PET than the other scenarios including the control.

3.3 Caveats

Results presented here are likely dependent on the baseline land cover of the neighborhood under investigation. This is because baseline land cover dictates the extent to which land cover change can be implemented. For example, a neighborhood that contains many homes with cool roofs and street trees will benefit less from these strategies. As another example, neighborhoods in which pavements are fully shaded by street trees will likely show negligible impacts from cool pavements. In addition, results are likely dependent on the baseline meteorology of the neighborhood. We recommend future studies that investigate the efficacy of different heat mitigation strategies in a variety of neighborhoods and baseline meteorological conditions.

The calculation of thermal comfort was based on an average adult male walking (80 W) in the neighborhood with summer clothing (0.5 Clo). The results reported here may depend on assumed pedestrian characteristics such as gender, age, height, weight, activity level, and clothing properties. These parameters can change metabolism and radiation exchange of the pedestrian with surroundings. In addition, we focus only on thermal comfort of outdoor pedestrians and do not consider indoor thermal comfort. Cool roofs, green roofs, and trees that shade buildings can reduce indoor air temperatures of unconditioned spaces and therefore improve indoor thermal comfort as well [70-72].

It is also important to note that, as with any study that relies on a numerical model, results and conclusions can be dependent on the particular model used. For example, the model used here may not adequately resolve the shedding of turbulent eddies around buildings, which may lead to less coupling between roofs and the near-ground environment than occurs in reality. We suggest future work investigate the model dependence of the research presented here.

Lastly, results presented here may be dependent on the particular receptor locations chosen.

4- Summary and Conclusions

In this study, the impacts of four heat mitigation strategies on the thermal comfort of pedestrians was assessed for a neighborhood in the city of El Monte, located in eastern Los Angeles County. The four strategies included solar reflective “cool” roofs, vegetative “green roofs”, solar reflective cool pavements, and increased street-level urban vegetation. The impacts of these strategies on local surface air and mean radiant temperature were simulated using a micrometeorological model. The simulations were performed for a summer day during a heat wave in July 2014. Physiological Equivalent Temperature (PET) was computed using RayMan to quantify thermal comfort of pedestrians for each heat mitigation strategy scenario. Increases in PET are associated with decreased thermal comfort.

Comparison of the results of these scenarios with the control scenario assuming current land cover in the neighborhood showed that converting existing streets to cool pavements could appreciably reduce surface air temperatures in the neighborhood. Adding street-level trees were also found to decrease surface air temperatures, though to a lesser extent than cool pavements. Cool and green roofs were found to have small impacts on surface air temperatures relative to cool pavements and street trees. This is due to the fact that they modify the energy budget at roof level and not at ground level.

Mean radiant temperatures at the mean height of pedestrians (1.5m) were computed at 10 receptor locations within the neighborhood, five of which were unshaded and above pavements, and five of which were underneath trees (near pavements) and thus shaded. Though cool pavements were found to reduce surface air temperatures in the unshaded receptors, they also increased mean radiant temperature at the mean height of pedestrians (1.5m) during the day. This occurred due to the increase in reflected shortwave radiation at the surface. Cool pavements subsequently increased PET in the unshaded receptor locations, and therefore reduced the thermal comfort of pedestrians during the day. In the shaded receptor locations, cool pavements caused reductions in surface air temperatures but small changes in mean radiant temperature during the day. The air temperature effect outweighed the radiative effect, and cool pavements therefore decreased PET at the shaded receptors. Cool pavements also absorbed less heat during the day and therefore released less at night, leading to reductions in nighttime surface air temperatures and PET.

In contrast, adding street trees led to relatively small reductions in surface air temperature and mean radiant temperature in both unshaded and shaded receptor locations, where shaded

receptor locations were underneath trees that existed in the control. PET was decreased and thermal comfort was improved at all receptors. Thermal comfort improvements from trees were more pronounced when comparing shaded to unshaded receptors.

Cool and green roofs led to small changes in surface air temperature, mean radiant temperature, and consequently thermal comfort, due to the fact that these strategies modify the energy balance at roof level, well above the height of pedestrians.

In this study we investigate the efficacy with which adopting heat mitigation strategies at the neighborhood scale could modify microclimate and the thermal comfort of pedestrians. Future work should investigate how results presented here vary depending on the baseline climate, baseline land cover, and numerical model used. Investigating the impacts of these heat mitigation strategies on indoor thermal comfort, as well as building energy use, is also of interest.

Acknowledgements

This research was funded by the National Science Foundation under grant CBET-1512429. It was also funded in part by the Rose Hills Foundation and the USC Provost's Office.

References

1. UN. *United Nation Population Division*. 2009.
2. Howard, L., *The climate of London, deduced from meteorological observations made in the metropolis and various places around it*. 1833, London: Harvey and Darton.
3. Oke, T.R., *Boundary Layer Climates*. 1987, New York: Routledge.
4. Grimmond, C.S.B. and Oke, T.R., *An evapotranspiration-interception model for urban areas*. Water Resources Research, 1991. **27**(7): p. 1739-1755.
5. Sailor, D.J., *Simulations of annual degree day impacts of urban vegetative augmentation*. Atmospheric Environment, 1998. **32**(1): p. 43-52.
6. Yang, F., Lau, S.S.Y., and Qian, F., *Urban design to lower summertime outdoor temperatures: An empirical study on high-rise housing in Shanghai*. Building and Environment, 2011. **46**(3): p. 769-785.
7. Sailor, D.J. and Fan, H., *The importance of including anthropogenic heating in mesoscale modeling of the urban heat island*, in *84th annual meeting of the AMS, Symposium on Planning, Nowcasting, and Forecasting in the Urban Zone*. 2004: Seattle.
8. Offerle, B., Grimmond, C.S.B., and Fortuniak, K., *Heat storage and anthropogenic heat flux in relation to the energy balance of a central European city centre*. International Journal of Climatology, 2005. **25**(10): p. 1405-1419.

9. Hamilton, I.G., Davies, M., Steadman, P., Stone, A., Ridley, I., and Evans, S., *The significance of the anthropogenic heat emissions of London's buildings: A comparison against captured shortwave solar radiation*. *Building and Environment*, 2009. **44**(4): p. 807-817.
10. Sailor, D.J., *Urban heat islands, Opportunities and challenges for mitigation and adaptation, in North American Urban Heat Island Summit*. 2002: Toronto, Canada.
11. McGugan, E.A., *Hyperpyrexia in the emergency department*. *Emergency Medicine*, 2001. **13**(1): p. 116-120.
12. Akbari, H. and Matthews, H.D., *Global cooling updates: Reflective roofs and pavements*. *Energy and Buildings*, 2012. **55**(0): p. 2-6.
13. Rosenfeld, A.H., Akbari, H., Bretz, S., Fishman, B.L., Kurn, D.M., Sailor, D., and Taha, H., *Mitigation of urban heat islands: materials, utility programs, updates*. *Energy and Buildings*, 1995. **22**(3): p. 255-265.
14. Akbari, H. and Konopacki, S., *Calculating energy-saving potentials of heat-island reduction strategies*. *Energy Policy*, 2005. **33**(6): p. 721-756.
15. Akbari, H., Menon, S., and Rosenfeld, A., *Global cooling: increasing world-wide urban albedos to offset CO₂*. *Climatic Change*, 2009. **94**(3-4): p. 275-286.
16. Hashem Akbari, Ryan Bell, Tony Brazel, David Cole, Maury Estes, Gordon Heisler, . . . Zalph, B., *Reducing Urban Heat Islands: Compendium of Strategies*. 2008, United States Environmental Protection Agency.
17. Georgescu, M., Morefield, P.E., Bierwagen, B.G., and Weaver, C.P., *Urban adaptation can roll back warming of emerging megapolitan regions*. *Proceedings of the National Academy of Sciences*, 2014. **111**(8): p. 2909-2914.
18. Georgescu, M., Mahalov, A., and Moustou, M., *Seasonal hydroclimatic impacts of Sun Corridor expansion*. *Environmental Research Letters*, 2012. **7**(3): p. 034026.
19. Georgescu, M., Moustou, M., Mahalov, A., and Dudhia, J., *Summer-time climate impacts of projected megapolitan expansion in Arizona*. *Nature Clim. Change*, 2013. **3**(1): p. 37-41.
20. Dan, L., Bou-Zeid, E., and Oppenheimer, M., *The effectiveness of cool and green roofs as urban heat island mitigation strategies*. *Environmental Research Letters*, 2014. **9**(5): p. 055002.
21. Li, D. and Bou-Zeid, E., *Quality and sensitivity of high-resolution numerical simulation of urban heat islands*. *Environmental Research Letters*, 2014. **9**(5): p. 055001.
22. Li, D., Sun, T., Liu, M., Yang, L., Wang, L., and Gao, Z., *Contrasting responses of urban and rural surface energy budgets to heat waves explain synergies between urban heat islands and heat waves*. *Environmental Research Letters*, 2015. **10**(5): p. 054009.
23. Lynn, B.H., Carlson, T.N., Rosenzweig, C., Goldberg, R., Druyan, L., Cox, J., . . . Civerolo, K., *A Modification to the NOAA LSM to Simulate Heat Mitigation Strategies in the New York City Metropolitan Area*. *Journal of Applied Meteorology and Climatology*, 2009. **48**(2): p. 199-216.
24. Taha, H., *Meso-urban meteorological and photochemical modeling of heat island mitigation*. *Atmospheric Environment*, 2008. **42**(38): p. 8795-8809.
25. Taha, H., *Episodic Performance and Sensitivity of the Urbanized MM5 (uMM5) to Perturbations in Surface Properties in Houston Texas*. *Boundary-Layer Meteorology*, 2008. **127**(2): p. 193-218.
26. Taha, H., Konopacki, S., and Gaberseck, S., *Impacts of Large-Scale Surface Modifications on Meteorological Conditions and Energy Use: A 10-Region Modeling Study*. *Theoretical and Applied Climatology*, 1999. **62**(3-4): p. 175-185.
27. Taha, H., Akbari, H., Rosenfeld, A., and Huang, J., *Residential cooling loads and the urban heat island—the effects of albedo*. *Building and Environment*, 1988. **23**(4): p. 271-283.
28. Ban-Weiss, G.A., Woods, J., Millstein, D., and Levinson, R., *Using remote sensing to quantify albedo of roofs in seven California cities, Part 2: Results and application to climate modeling*. *Solar Energy*, 2015. **115**(0): p. 791-805.

29. Middel, A., Chhetri, N., and Quay, R., *Urban forestry and cool roofs: Assessment of heat mitigation strategies in Phoenix residential neighborhoods*. Urban Forestry & Urban Greening, 2015. **14**(1): p. 178-186.
30. Nazarian, N. and Kleissl, J., *CFD simulation of an idealized urban environment: Thermal effects of geometrical characteristics and surface materials*. Urban Climate, 2015. **12**(0): p. 141-159.
31. Yaghoobian, N. and Kleissl, J., *Effect of reflective pavements on building energy use*. Urban Climate, 2012. **2**(0): p. 25-42.
32. Taleghani, M., Sailor, D.J., Tenpierik, M., and van den Dobbelsteen, A., *Thermal assessment of heat mitigation strategies: The case of Portland State University, Oregon, USA*. Building and Environment, 2014. **73**: p. 138-150.
33. Taleghani, M., Kleerekoper, L., Tenpierik, M., and van den Dobbelsteen, A., *Outdoor thermal comfort within five different urban forms in the Netherlands*. Building and Environment. **In Press**.
34. Johansson, E. and Emmanuel, R., *The influence of urban design on outdoor thermal comfort in the hot, humid city of Colombo, Sri Lanka*. International Journal of Biometeorology, 2006. **51**(2): p. 119-133.
35. Santamouris, M., *Cooling the cities – A review of reflective and green roof mitigation technologies to fight heat island and improve comfort in urban environments*. Solar Energy, 2014. **103**: p. 682-703.
36. Millstein, D. and Menon, S., *Regional climate consequences of large-scale cool roof and photovoltaic array deployment*. Environmental Research Letters, 2011. **6**(3): p. 034001.
37. Taha, H., *Urban Surface Modification as a Potential Ozone Air-quality Improvement Strategy in California: A Mesoscale Modelling Study*. Boundary-Layer Meteorology, 2008. **127**(2): p. 219-239.
38. Matzarakis, A. and Amelung, B., *Physiological Equivalent Temperature as Indicator for Impacts of Climate Change on Thermal Comfort of Humans*, in *Seasonal Forecasts, Climatic Change and Human Health*, Thomson, M.C., García Herrera, R. and Beniston, M., Editors. 2008, Springer.
39. Höpfe, P., *The physiological equivalent temperature - A universal index for the biometeorological assessment of the thermal environment*. International Journal of Biometeorology, 1999. **43**(2): p. 71-75.
40. Matzarakis, A., *Influence of mean radiant temperature on thermal comfort of humans in idealized urban environments in Ninth Symposium on the Urban Environment*. 2010: Keystone (CO), United States.
41. Thorsson, S., Lindberg, F., Eliasson, I., and Holmer, B., *Different methods for estimating the mean radiant temperature in an outdoor urban setting*. International Journal of Climatology, 2007. **27**(14): p. 1983-1993.
42. Thorsson, S., Rocklöv, J., Konarska, J., Lindberg, F., Holmer, B., Dousset, B., and Rayner, D., *Mean radiant temperature – A predictor of heat related mortality*. Urban Climate, 2014. **10**, Part **2**(0): p. 332-345.
43. ISO7726, *International Standard 7726*, in *Ergonomics of the thermal environment - Instrument for measuring physical quantities*. 1998, ISO Geneva.
44. Spronken-Smith, R.A. and Oke, T.R., *The thermal regime of urban parks in two cities with different summer climates*. International Journal of Remote Sensing, 1998. **19**(11): p. 2085-2104.
45. Shashua-Bar, L. and Hoffman, M.E., *Vegetation as a climatic component in the design of an urban street: An empirical model for predicting the cooling effect of urban green areas with trees*. Energy and Buildings, 2000. **31**(3): p. 221-235.
46. Shashua-Bar, L., Pearlmutter, D., and Erell, E., *The cooling efficiency of urban landscape strategies in a hot dry climate*. Landscape and Urban Planning, 2009. **92**(3-4): p. 179-186.

47. Lin, B.-S. and Lin, Y.-J., *Cooling Effect of Shade Trees with Different Characteristics in a Subtropical Urban Park*. HortScience, 2010. **45**(1): p. 83-86.
48. Synnefa, A., Dandou, A., Santamouris, M., Tombrou, M., and Soulakellis, N., *On the Use of Cool Materials as a Heat Island Mitigation Strategy*. Journal of Applied Meteorology and Climatology, 2008. **47**(11): p. 2846-2856.
49. Zhou, Y. and Shepherd, J.M., *Atlanta's urban heat island under extreme heat conditions and potential mitigation strategies*. Natural Hazards, 2010. **52**(3): p. 639-668.
50. Ban-Weiss, G.A., Woods, J., and Levinson, R., *Using remote sensing to quantify albedo of roofs in seven California cities, Part 1: Methods*. Solar Energy, 2015. **115**(0): p. 777-790.
51. Santamouris, M., Gaitani, N., Spanou, A., Saliari, M., Giannopoulou, K., Vasilakopoulou, K., and Kardomateas, T., *Using cool paving materials to improve microclimate of urban areas – Design realization and results of the flisvos project*. Building and Environment, 2012. **53**(0): p. 128-136.
52. Bruse, M. and Fleer, H., *Simulating surface–plant–air interactions inside urban environments with a three dimensional numerical model*. Environmental Modelling & Software, 1998. **13**(3–4): p. 373-384.
53. Yamada, T. and Mellor, G., *A Simulation of the Wangara Atmospheric Boundary Layer Data*. Journal of the Atmospheric Sciences, 1975. **32**(12): p. 2309-2329.
54. Liu, J., Chen, J.M., Black, T.A., and Novak, M.D., *E-ε modelling of turbulent air flow downwind of a model forest edge*. Boundary-Layer Meteorology, 1996. **77**(1): p. 21-44.
55. Wilson, J.D., *A second-order closure model for flow through vegetation*. Boundary-Layer Meteorology, 1988. **42**(4): p. 371-392.
56. Bruse, M., *Development of a microscale model for the calculation of surface temperatures in structured terrain*. 1995, Inst. for Geography, Univ. Bochum.
57. Bruse, M., *ENVI-met 3.0: Updated Model Overview*. 2004.
58. Kottek, M., Grieser, J., Beck, C., Rudolf, B., and Rubel, F., *World Map of the Köppen-Geiger climate classification updated*. Meteorologische Zeitschrift, 2006. **15**(3).
59. www.weather.com. [cited 2015; Available from: <http://www.weather.com>].
60. United States Census Bureau. *El Monte (city) QuickFacts*. 2010 09.28.2015]; Available from: <http://quickfacts.census.gov/qfd/states/06/0622230.html>.
61. Sleiman, M., Ban-Weiss, G., Gilbert, H.E., François, D., Berdahl, P., Kirchstetter, T.W., . . . Levinson, R., *Soiling of building envelope surfaces and its effect on solar reflectance—Part I: Analysis of roofing product databases*. Solar Energy Materials and Solar Cells, 2011. **95**(12): p. 3385-3399.
62. *The Cool Roof Rating Council*. [cited 2015; Available from: <http://www.coolroofs.org/>].
63. ISO, *International Standard 7730*. 1984, ISO Geneva, revised 1990.
64. Höpfe, P., *Heat balance modelling*. Experientia, 1993. **49**(9): p. 741-746.
65. Matzarakis, A., Mayer, H., and Iziomon, M.G., *Applications of a universal thermal index: physiological equivalent temperature*. International Journal of Biometeorology, 1999. **43**(2): p. 76-84.
66. Blazejczyk, K., Epstein, Y., Jendritzky, G., Staiger, H., and Tinz, B., *Comparison of UTCI to selected thermal indices*. International Journal of Biometeorology, 2012. **56**(3): p. 515-535.
67. Matzarakis, A., Rutz, F., and Mayer, H., *Modelling the thermal bioclimate in urban areas with the RayMan Model*, in *PLEA2006 - The 23rd Conference on Passive and Low Energy Architecture*. 2006: Geneva, Switzerland.
68. ASHRAE, *ASHRAE Standard 55–2010 in Thermal Environmental Conditions for Human Occupancy*. 2010, ASHRAE Atlanta, GA.
69. Botham-Myint, D., Recktenwald, G.W., and Sailor, D.J., *Thermal footprint effect of rooftop urban cooling strategies*. Urban Climate.

70. Synnefa, A., Santamouris, M., and Akbari, H., *Estimating the effect of using cool coatings on energy loads and thermal comfort in residential buildings in various climatic conditions*. Energy and Buildings, 2007. **39**(11): p. 1167-1174.
71. Morakinyo, T.E., Adegun, O.B., and Balogun, A.A., *The effect of vegetation on indoor and outdoor thermal comfort conditions: Evidence from a microscale study of two similar urban buildings in Akure, Nigeria*. Indoor and Built Environment, 2014.
72. Taleghani, M., Tenpierik, M., and van den Dobbelen, A., *Indoor thermal comfort in urban courtyard block dwellings in the Netherlands*. Building and Environment, 2014. **82**: p. 566-579.

Table 1: Assumed boundary conditions and building indoor temperatures and thermal properties

Simulation start time	30 July 2014, 4:00am
Simulation end time	31 July 2014, 4:00am
Size of grid cells (dx, dy, dz)	3m x 3m x 1m ^a
Initial temperature atmosphere	292.5 K
Wind speed at 2m	1.6 m/s
Wind direction	270° (West)
Relative humidity at 2m	81%
Building indoor temperature	20 °C

^a dz reported here is for the atmospheric surface layer. Vertical resolution becomes coarser with increasing altitude.

Table 2: Description of simulations.

Acronyms	Perturbation scenarios	Details
CO	Control	Represents current land cover characteristics
GR	Green roofs	Same as Control but rooftops were covered with grass.
CR	Cool roofs	Same as Control but albedo of the roofs were increased by 0.3 (from 0.1 to 0.4)
TA	Trees added	Same as Control but additional street trees were added in open grassy spaces adjacent to sidewalks and in front and backyards
CP	Cool pavement	Same as Control but the albedo of asphalt concrete pavements were increased by 0.3 (from 0.2 to 0.5).

Table 3: Thermal comfort ranges for physiological equivalent temperature (PET) [65].

PET (°C)	Thermal perception	Grade of physiological stress
T<4	Very cold	Extreme cold stress
4<T<8	Cold	Strong cold stress
8<T<13	Cool	Moderate cold stress
13<T<18	Slightly cool	Slightly cold stress
18<T<23	Comfortable	No thermal stress
23<T<29	Slightly warm	Slightly heat stress
29<T<35	Warm	Moderate heat stress
35<T<41	Hot	Strong heat stress
41<T	Very Hot	Extreme heat stress

Table 4: Conditions used in the simulation of thermal comfort using the RayMan model for a normal person.

Activity	80 W (walking)
Personal data	1.75m (height), 75kg, 35 years old, male
Clothing insulation	0.5 Clo (summer clothes)
Emission coefficient of the human body	Standard value 0.97



Figure 1: The neighborhood of focus in El Monte, California, located in eastern Los Angeles County. Red circles show unshaded and yellow circles show shaded receptor locations for the calculation of thermal comfort.

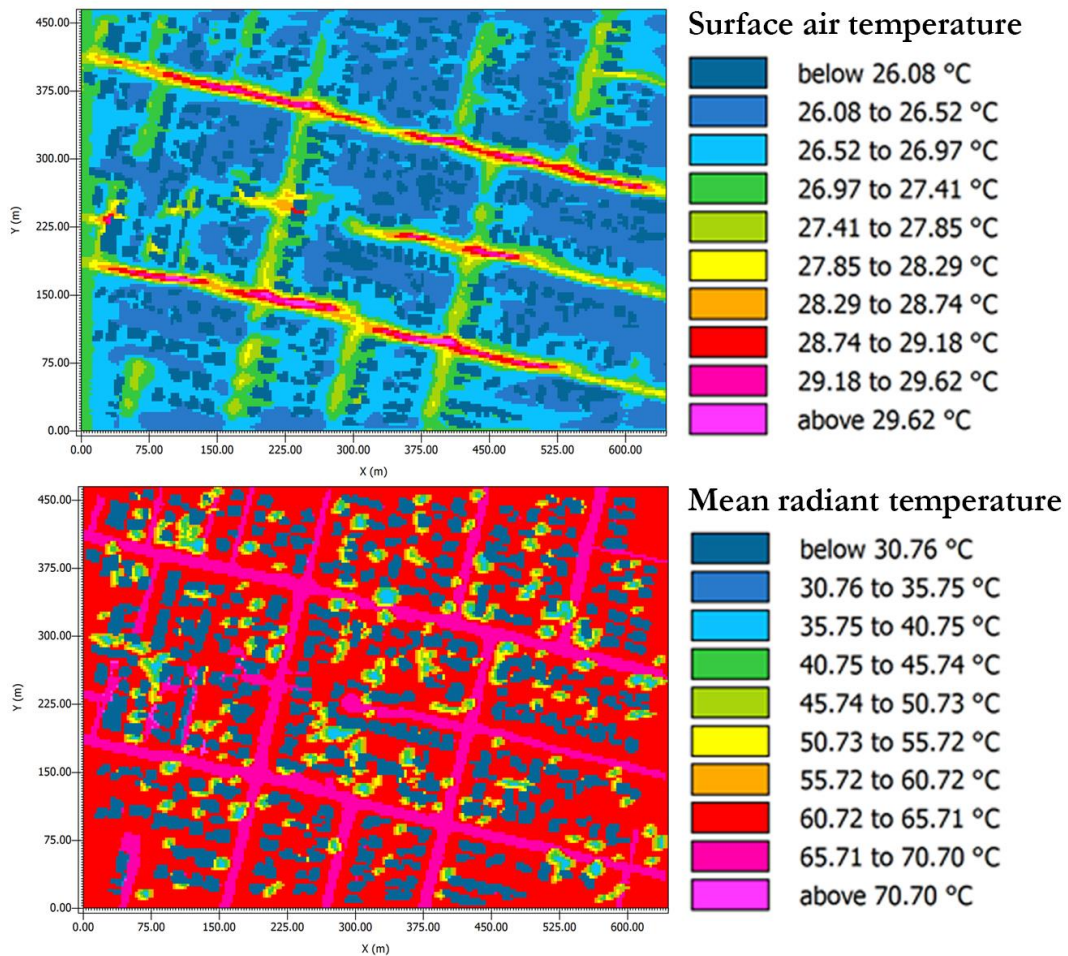


Figure 2: Surface air temperature (above) and mean radiant temperature (bottom) in the control simulation at 14:00h at a height of 1.5 m.

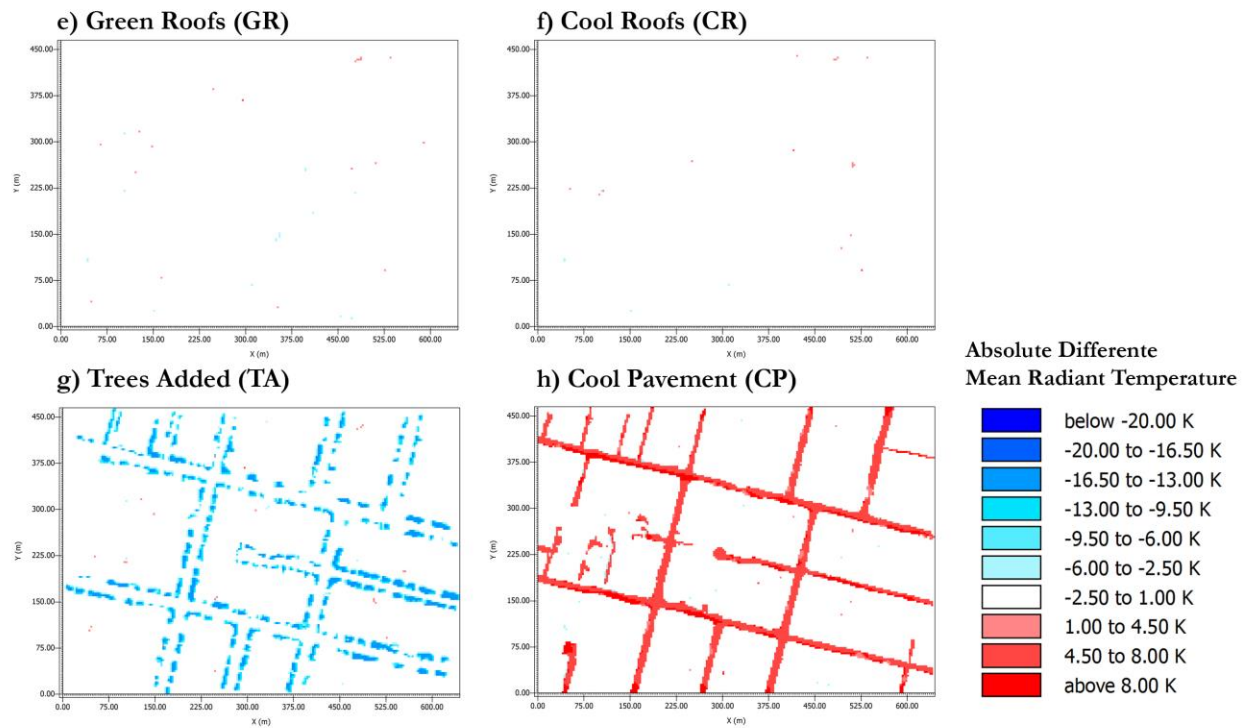
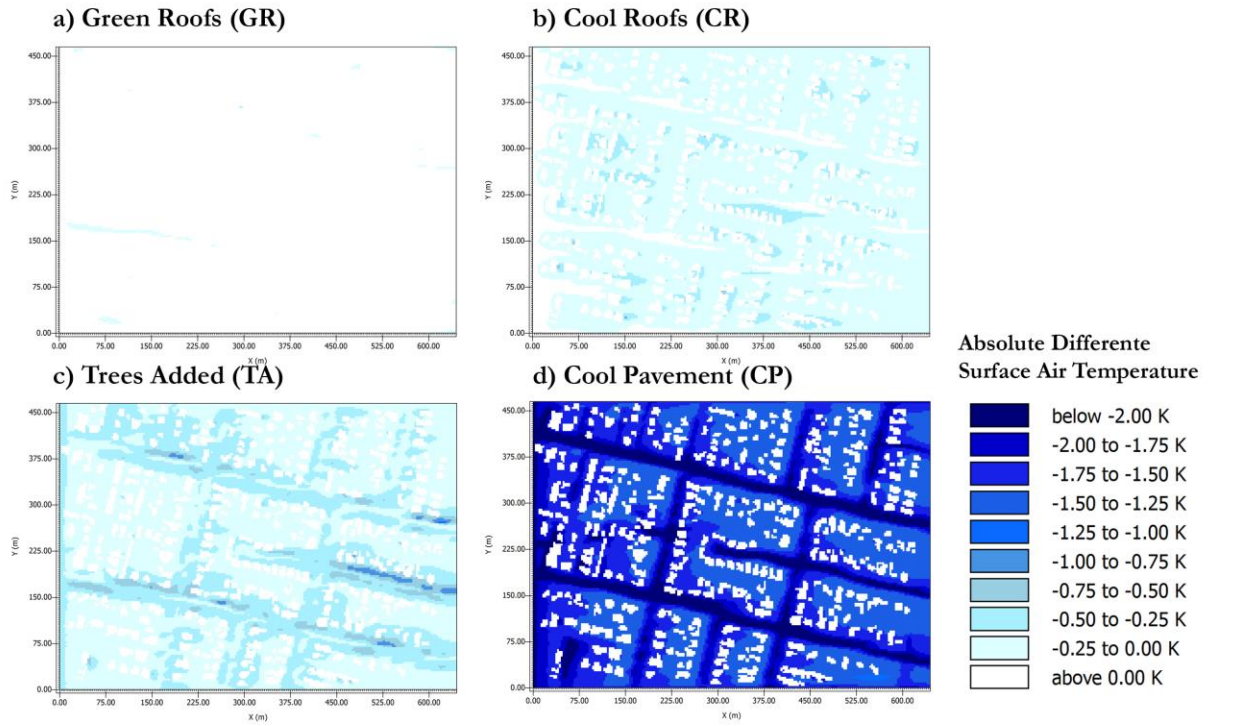


Figure 3: Change in surface air temperature (a-d) and mean radiant temperature (e-h) caused by the four heat mitigation strategies relative to the control simulation (perturbation minus control). Values are at 14:00 and at a height of 1.5m.

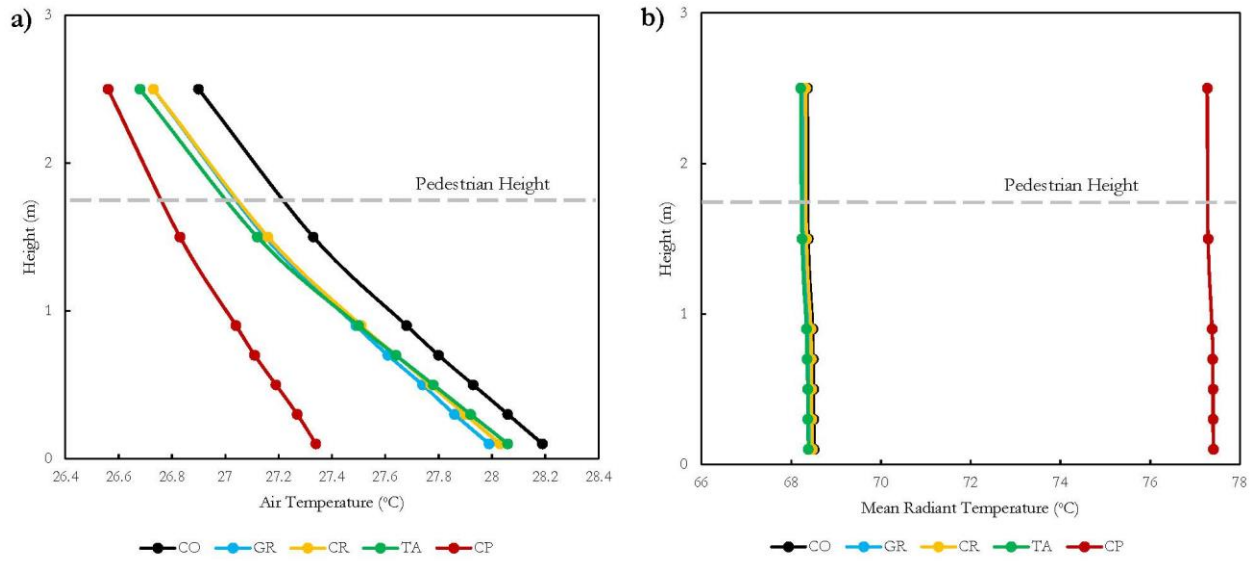


Figure 4: Vertical profiles of (a) air temperature and (b) mean radiant temperature at 14:00 for the unshaded receptor at the center of the model domain (see Figure 1).

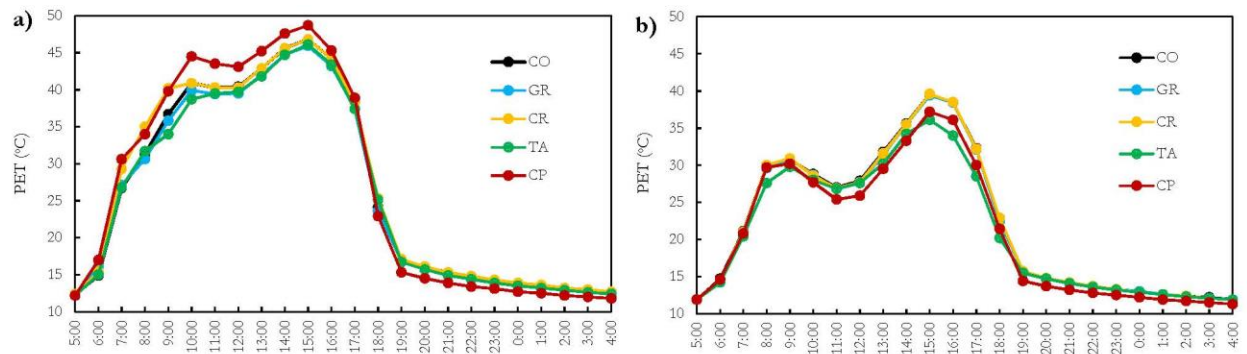


Figure 5: Diurnal profile of the mean physiological equivalent temperature for the five unshaded (a), and shaded (b) receptors.

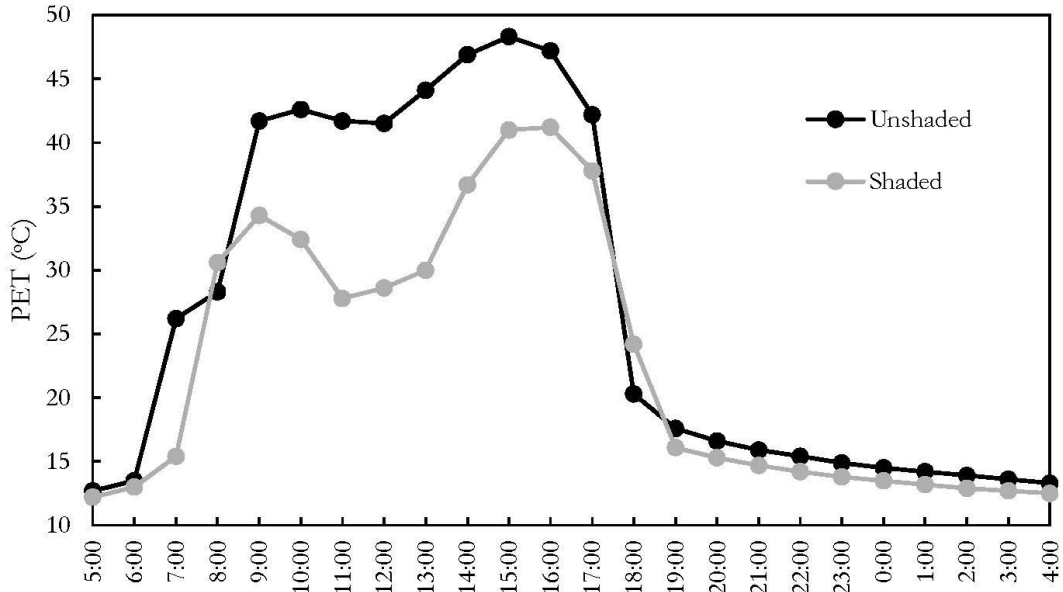


Figure 6: Diurnal profiles of physiological equivalent temperature in shaded and unshaded locations in the control simulation.

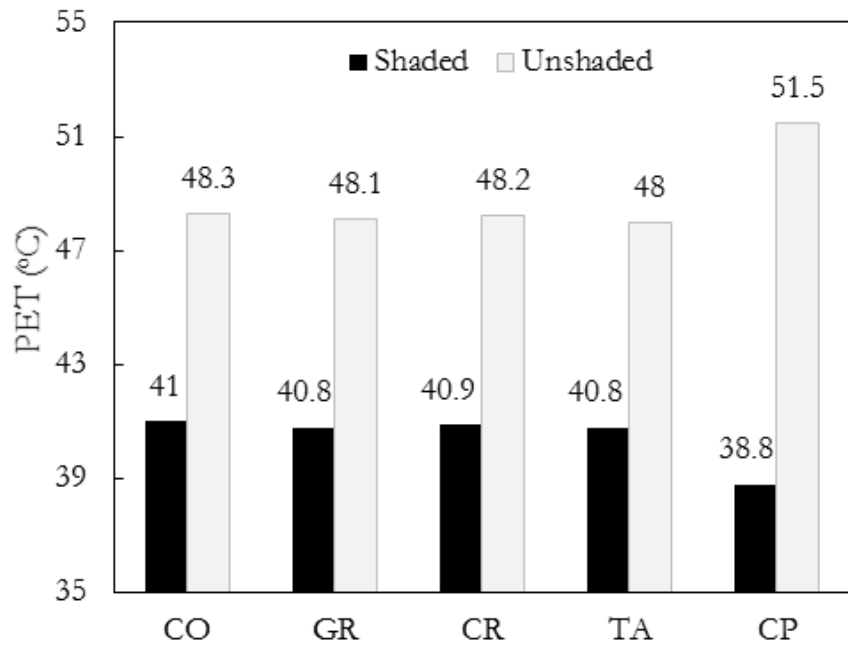


Figure 7: Comparison of PET in shaded and unshaded receptor locations in all scenarios at 15:00.